What is changing when: Decoding visual information in movies from human intracranial recordings

Leyla Isik[a,b], Jedediah Singer[b], Joseph R. Madsen[c], Nancy Kanwisher[b], and Gabriel Kreiman[a]

Supplementary Material

1. **Supplementary Figures**
2. **Supplementary Tables**
3. **Supplementary Discussion**

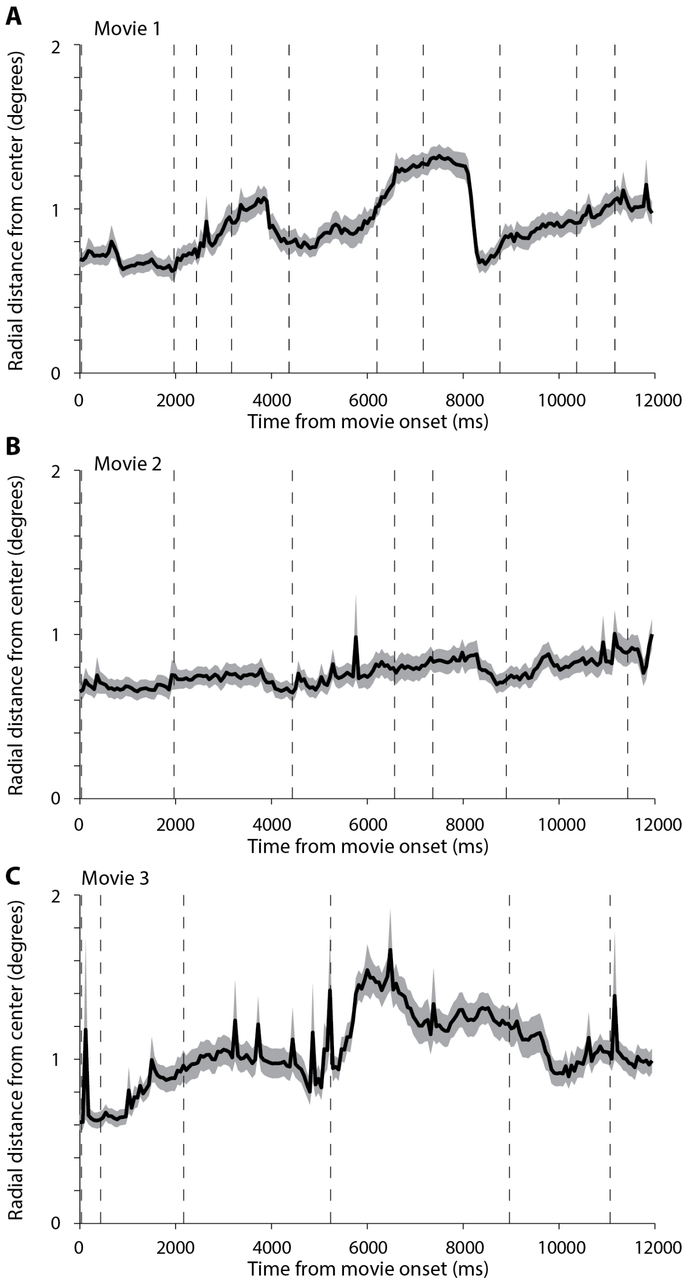

Supplemental Figure 1 – Experiment I, post-hoc eye tracking. Seven in-lab subjects watched 5 repetitions of the same 3 movie clips from Experiment I with the same stimulus presentation parameters while we performed eye tracking (~4x3 degree of visual angle movie clip presentation, **Methods**). We summarized eye positions here by reporting mean ± SEM across the repetitions and subjects for the radial distance from the eye position to the center of the screen. We calculated the median eye position per frame, and averaged the median eye position across all subjects and repetitions for each movie. We did not observe any systematic eye movements triggered by the movie cuts that were consistent across repetitions and subjects. Vertical lines denote movie cuts.

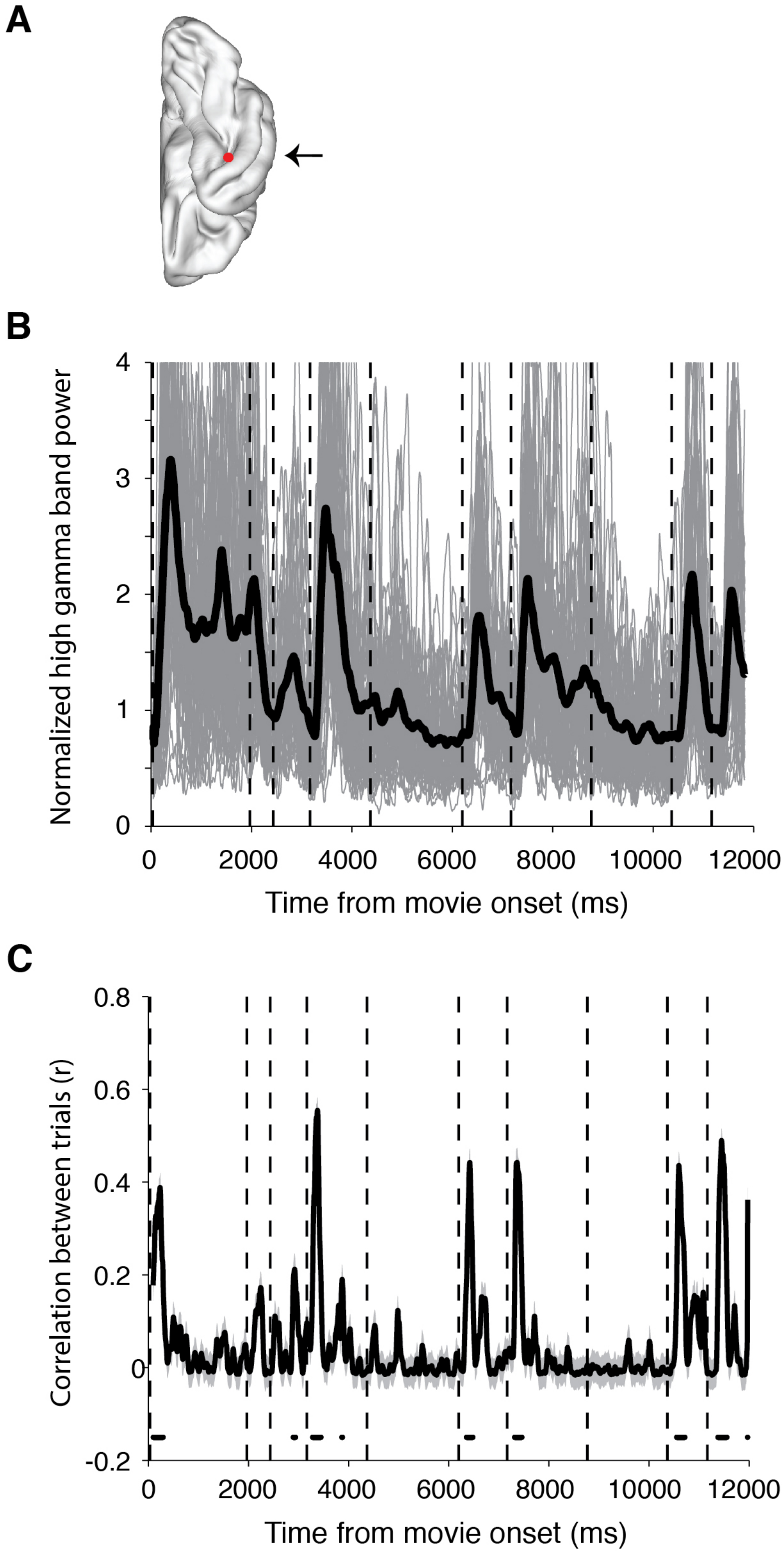

Supplemental Figure 2 - Example electrode showing high gamma band responses in Experiment I [expanding on Figure 2]
A. Location of an example cut-responsive electrode in the right middle occipital gyrus (Talairach coordinates = [53.4 -75.6 5.6]) based on responses filtered in the high gamma band (70-120 Hz). **B**. Normalized responses in the high gamma band over the entire 12 s movie clip 1. The format is the same as that in **Figure 2C**. High gamma power was normalized by dividing by the mean activity over the course of the entire 12 s clip. Mean activity across repetitions is shown with a thick black line, and individual repetitions (n=59) are shown with gray traces. Dashed vertical lines indicate movie cuts. **C**. Average correlation coefficient (Pearson coefficient, r, mean ± SEM) across the 59 choose 2 (1711) pairwise comparisons (calculated in 50ms non-overlapping bins). Horizontal black lines at the bottom of the plot indicate periods when the average pairwise correlation across repetitions was significantly above chance based on a p<0.01 permutation test (**Methods**).

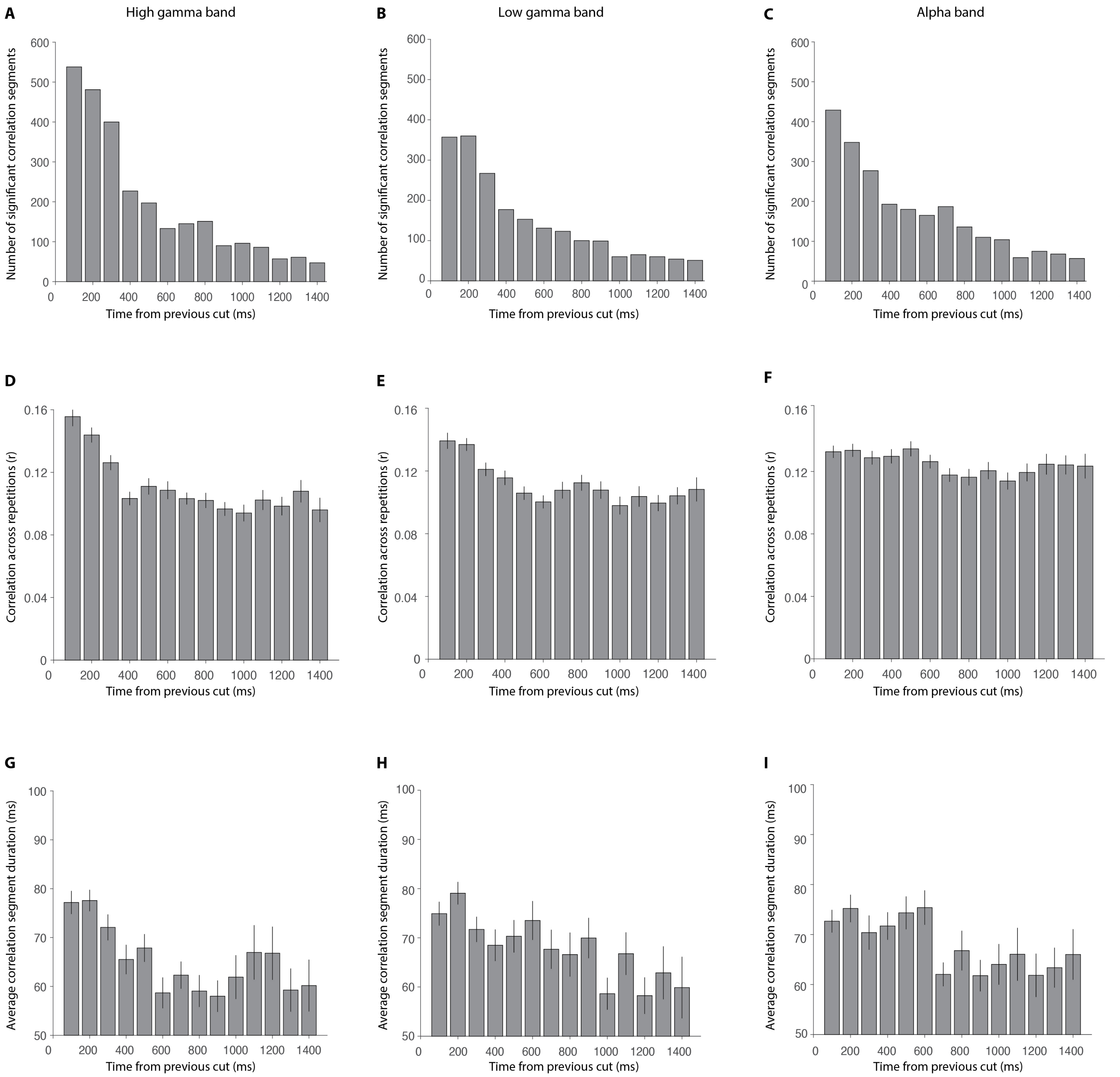

Supplemental Figure 3 – Properties of neural responses in different frequency bands that were consistent across trials [expanding on Figure 3]

A, B, C. Distribution of the onset of segments (of 50 ms duration) with significant correlation across repetitions based on the high gamma band (**A**), low gamma band (**B**), or alpha band (**C**), in all electrodes (n=954) as a function of time from the previous cut. Bin size = 100 ms. These segments of consistent correlation across repetitions begin mostly within the 300 ms following a cut.

D, E, F. Average correlation between repetitions in each time bin for all the segments with significant correlation between repetitions in **A**, **B, C** (mean±SEM).

G, H, I. Average duration of each segment for all the segments with significant correlation between repetitions in **A**, **B, C** (mean±SEM).

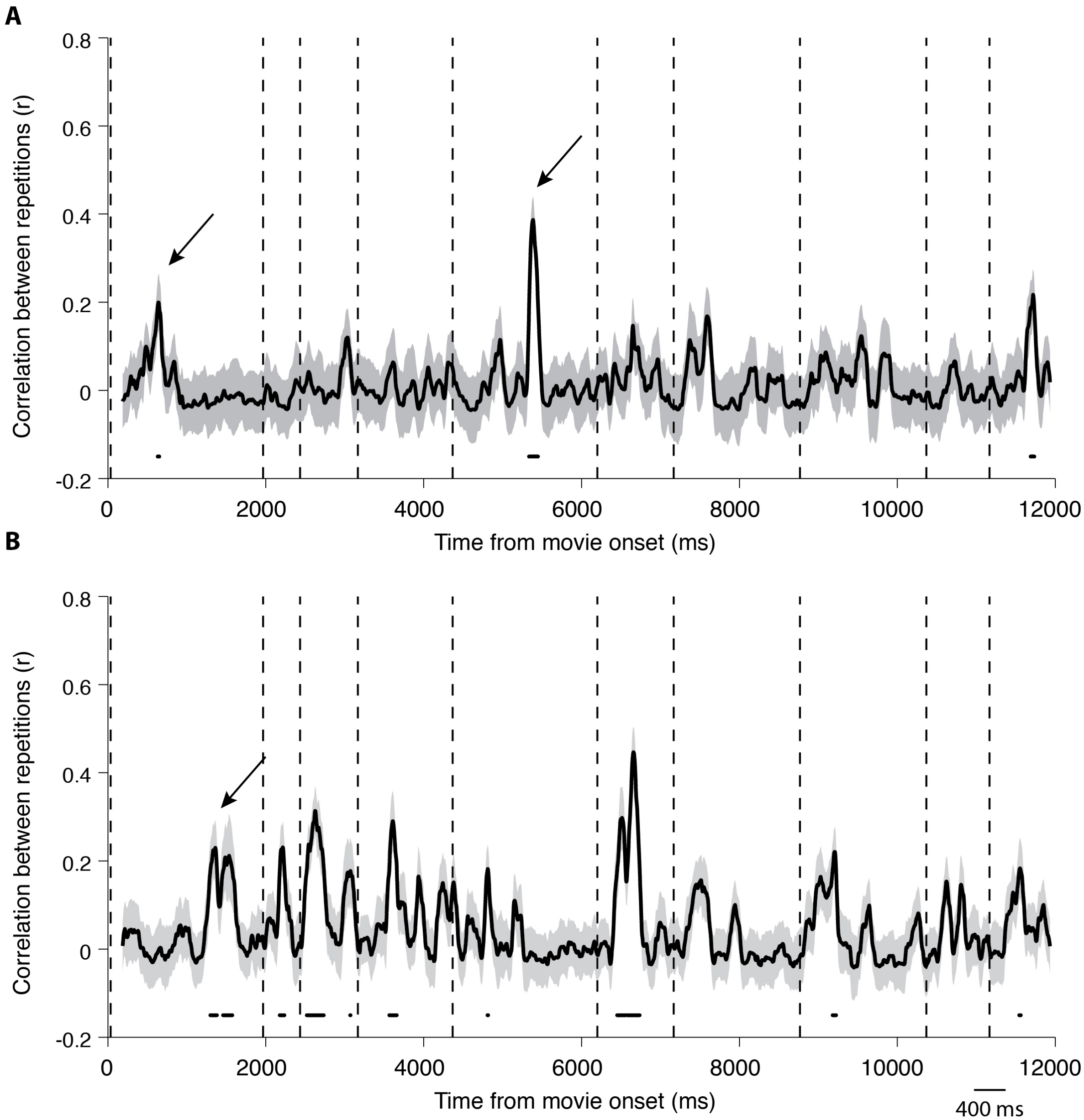

Supplemental Figure 4 – Consistent physiological responses during inter-movie cut periods in two example electrodes from two subjects [expanding on Figures 2-3]
Average pairwise correlation in the broadband signals across the 20 choose 2 (190) pairwise comparisons between repetitions (same format and conventions as **Figure 2C**). (**A**) Electrode located in left cuneus (Talairach coordinates = [-53.6 13.0 26.6]), and (**B**) electrode located in the right fusiform gyrus (Talairach coordinates = [-39.6 -59.0 -21.9]). The arrows point to segments with significant correlations that are >400 ms away from the preceding cut.

Supplemental Figure 5 – Maps of statistical significance of neural responses across movie repetitions [Expanding on Figure 3]
Locations of electrodes showing significant average pairwise correlations between repetitions calculated over the entire 12s clip. Electrode locations are projected on the Freesurfer fsaverage template brain (http://surfer.nmr.mgh.harvard.edu/), and shown at lateral, medial and ventral views for the left (left) and right (right) hemispheres. The color of each electrode denotes the p value for the statistical significance of the correlation coefficient (Methods, see color scale on bottom right) for (**A**) broadband, (**B**) high-gamma band, (**C**) low gamma band and (**D**) alpha band signals.

Figure S5A

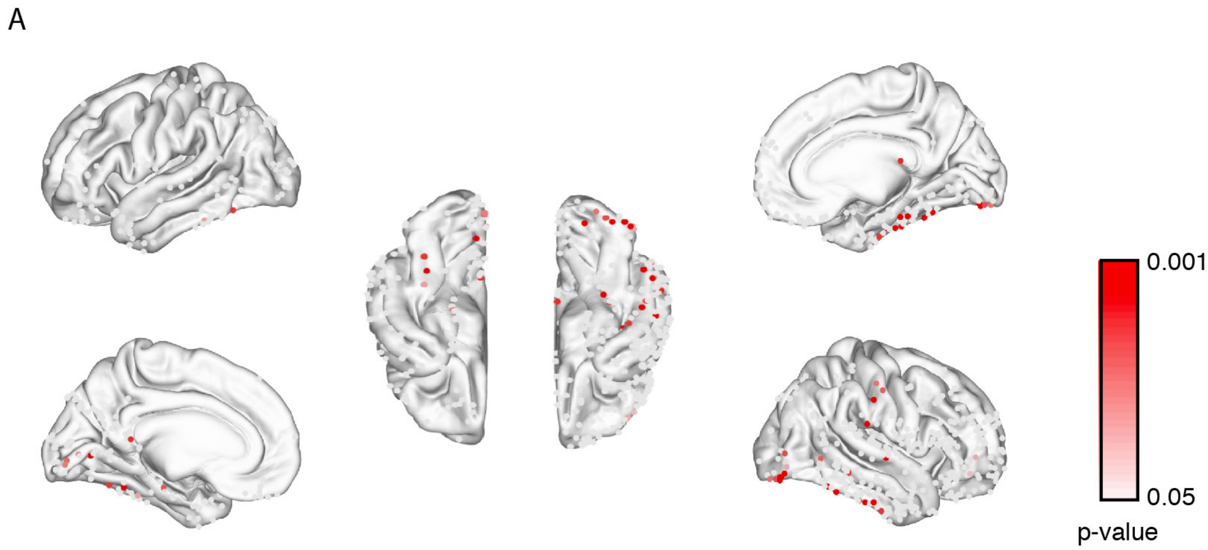

Figure S5B

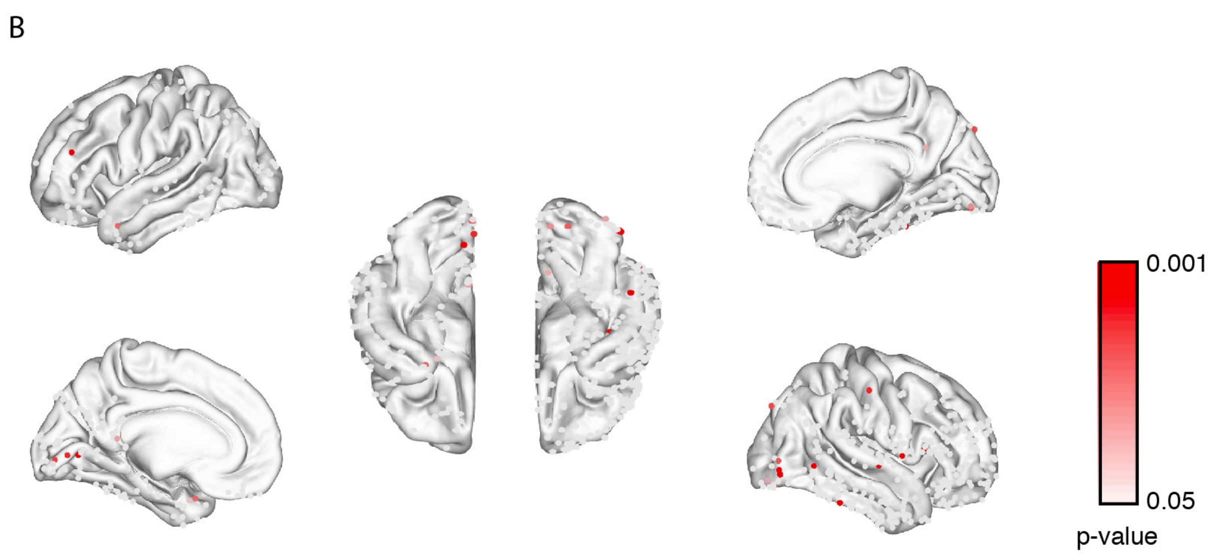

Figure S5C

C

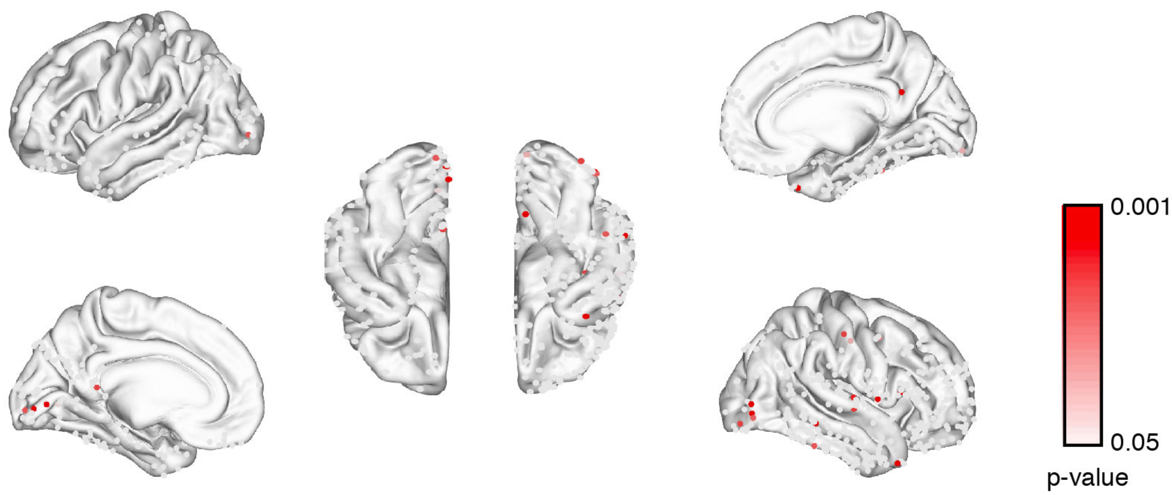

Figure S5D

D

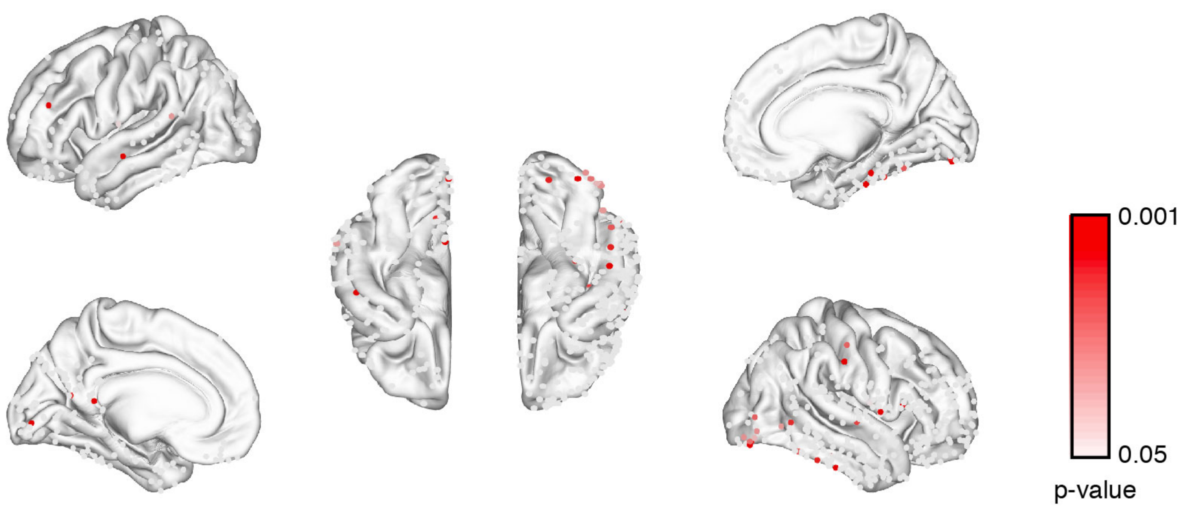

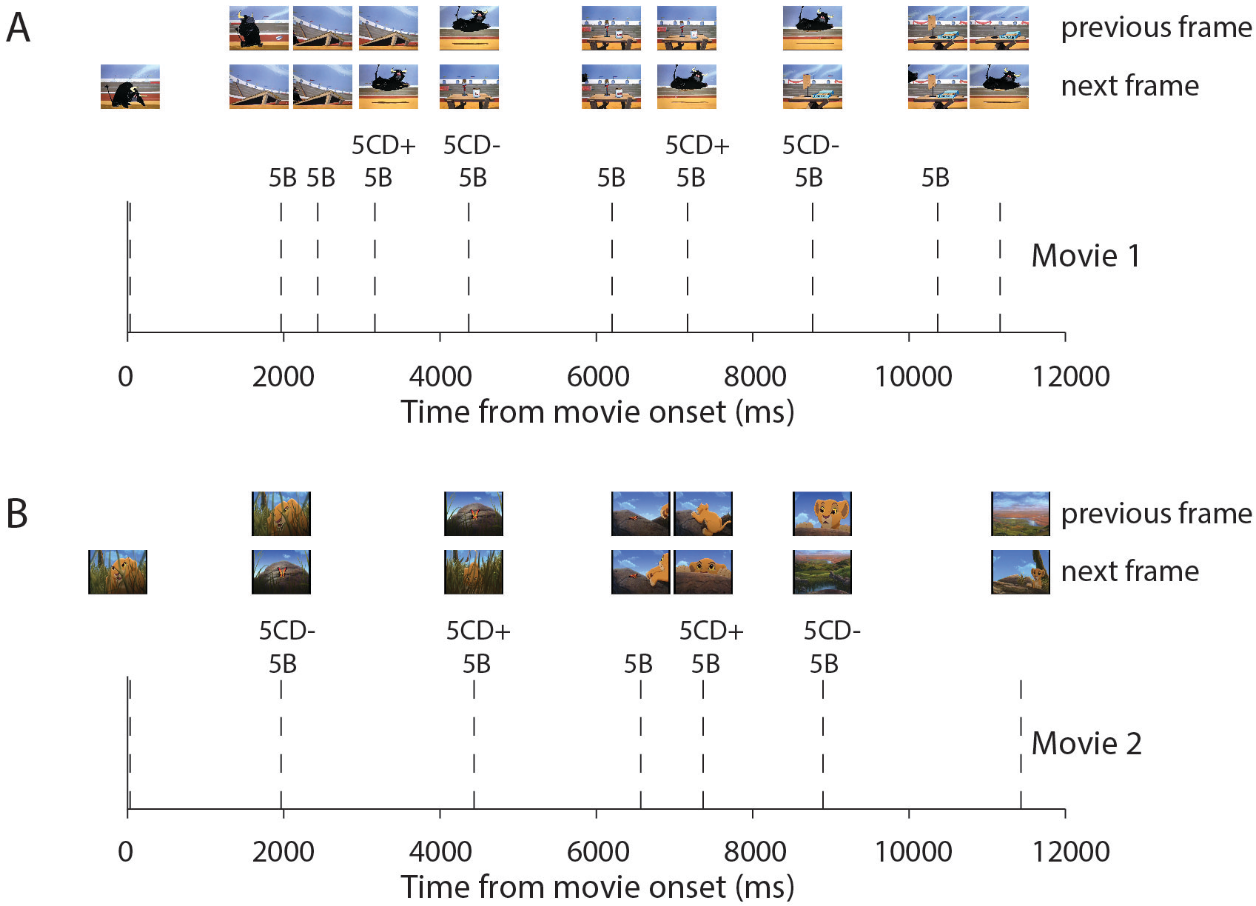

Supplemental Figure 6 – Definition of movie events for decoding analyses
This figure marks the movie cuts from Movie 1 (**A**) and Movie 2 (**B**) that were used in the decoding analyses (Experiment I). There were 13 movie cuts used in **Figure 5B** (all cuts, excluding the first and last to allow for a -200-1000 ms window around each cut), and 8 movie cuts used in **Figure 5C-D** (4 as positive examples, containing an animal, and 4 as negative examples, not containing an animal). For each of those events we show the frames preceding and right after the movie cut.

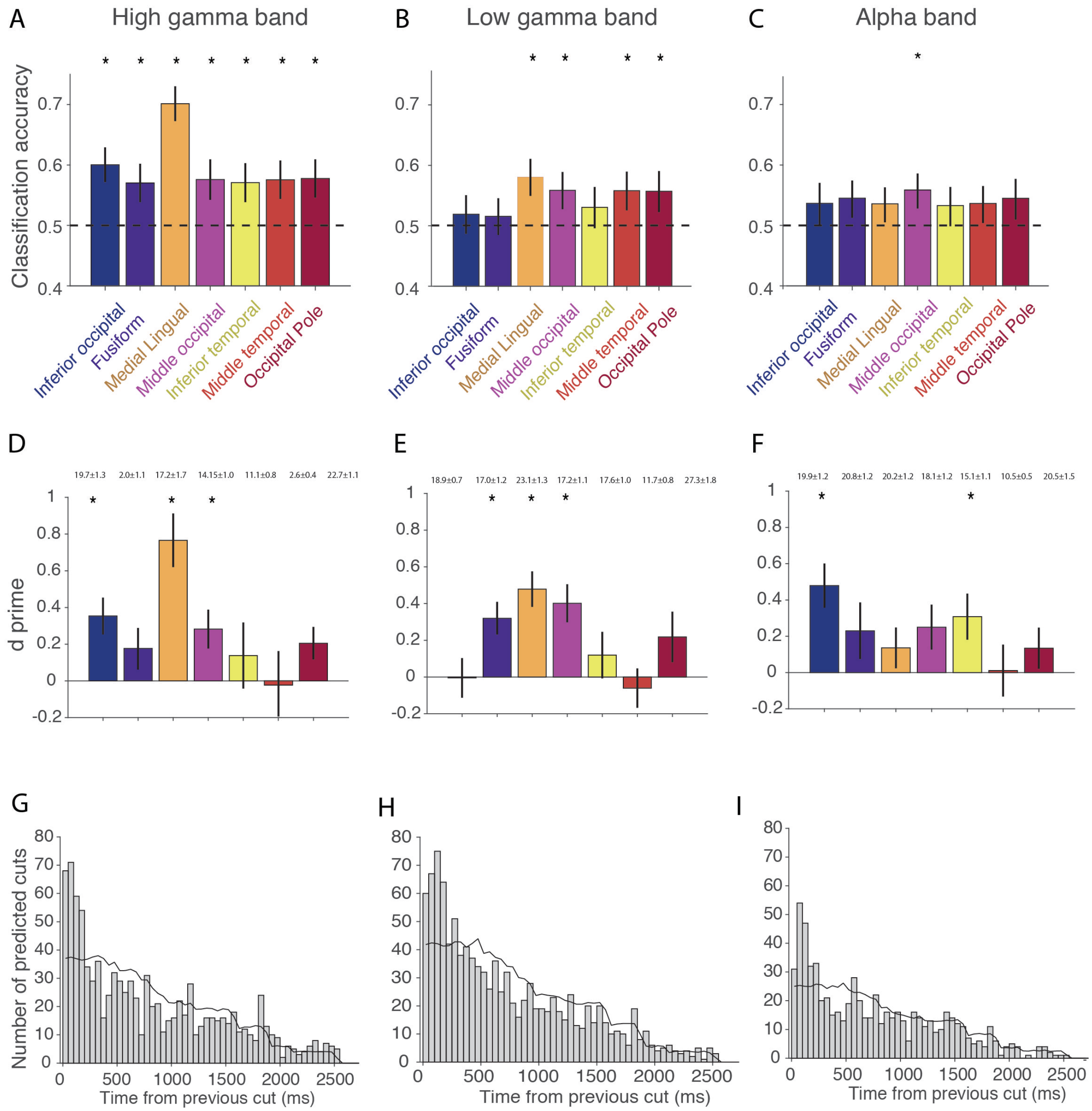

Supplemental Figure 7 – Decoding movie cuts and shots using other frequency bands in Experiment I [expanding on Figure 4]

This figure follows the format in **Figure 4**, using signals in the high gamma (70-120 Hz, **A, D, G, J**), low gamma (25-70 Hz, **B, E, H, K**) and alpha (8-15 Hz, **C, F, I, L**) frequency range.

(A-C) Classification accuracy from n=8 electrodes in each region between movie segments with a cut versus segments without a cut in the seven regions highlighted in **Figure 4A** (mean ± SD across 20 decoding runs). The classification accuracy is the average from 50-400 ms post cut onset. Asterisks indicate significant decoding for each of the decoding conditions based on a p<0.01 permutation test. Chance = 0.5, horizontal dashed line.

(D-F) Sensitivity (d') to detect visual transitions during the entire 12s clip time course for held out repetitions of movie clips 1 and 2 (mean ± SD across 20 decoding runs, Methods, **Figure**

S12B). Number at the top of each bar plot indicates the number of predicted cuts per region (the actual number of all cuts in movie clips 1 and 2 was 17).
(G-I) The bars show the latency difference between the time of the predicted visual transitions (first time point in “cut” predicted periods) in **D-F** and the time of the previous true cut for regions in each frequency band with significantly above chance d’ values in **D-F**. Bin size = 50 ms. The line shows the average distribution obtained from randomly selecting the same number of times as predicted visual transitions. The distribution of predicted visual transition times is significantly different than the random distribution with $p<10^{-7}$, $p<10^{-10}$, and $p<10^{-8}$, for high gamma, low gamma, and alpha bands, respectively, based on Kolmogorov-Smirnov test.

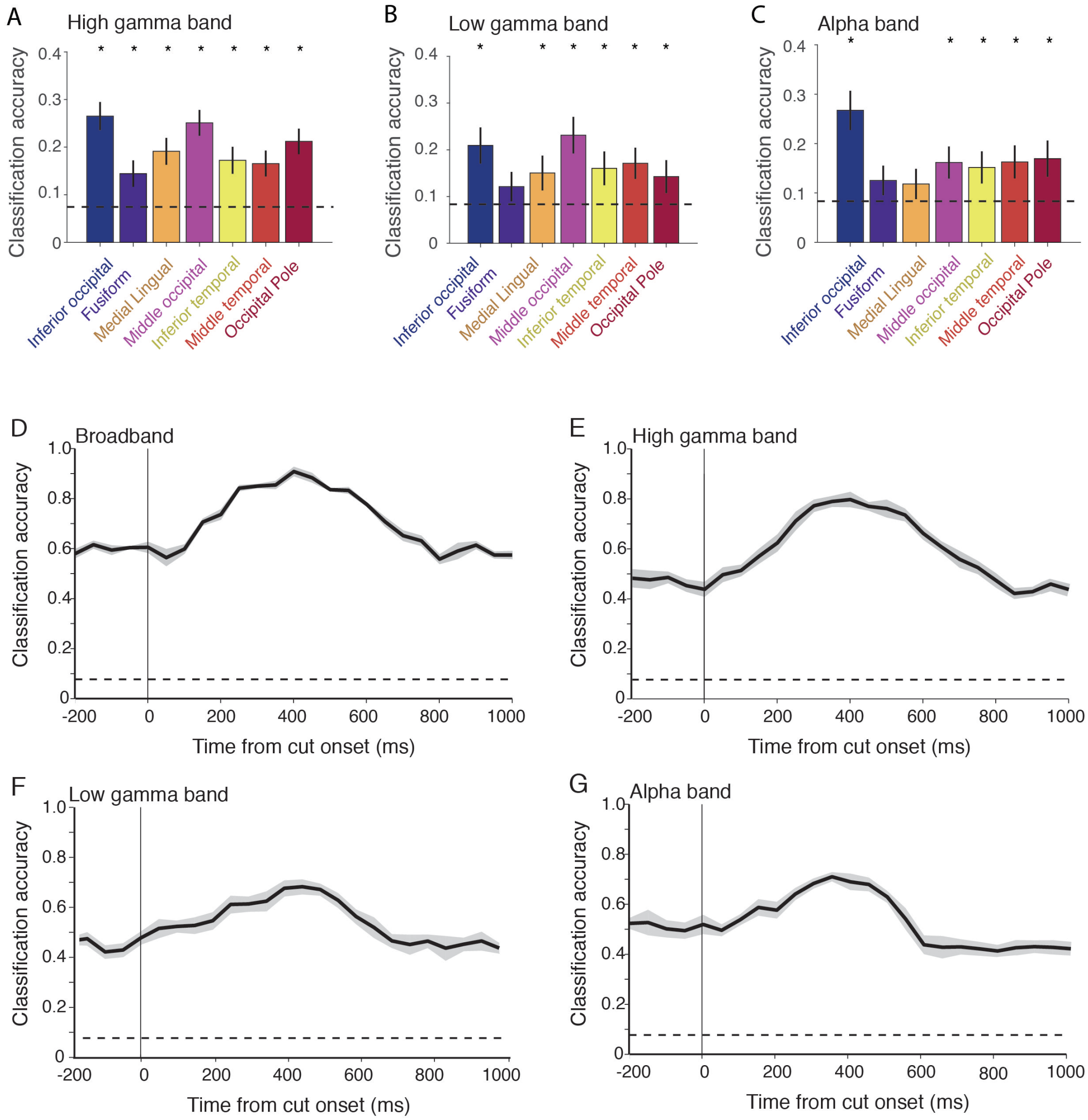

Supplemental Figure 8 – Event discrimination in different frequency bands and visualization of dynamic classification accuracy in Experiment I [expanding on Figure 5]. (A-C) Following the format in **Figure 5B**, using signals in the high gamma (70-120 Hz, **A**), low gamma (25-70 Hz, **B**) and alpha (8-15 Hz, **C**) frequency range. Classification accuracy to label each of the 13 cuts from clips 1 and 2 (**Fig. S6**) using n=8 electrodes in each of the seven regions highlighted in **Figure 4A** (mean ± SD across 20 decoding runs). Chance = 1/13, horizontal dashed line. The classification accuracy is reported as the average from 50-400 ms post cut onset. Asterisks indicate significant decoding based on a p<0.01 permutation test. (**D-G**) Classification accuracy versus time relative to cut onset for decoding among the 13 different shots from the pseudo population across all subjects, using broadband (**D**), high gamma band (**E**), low gamma band (**F**), or alpha band (**G**) signals as input to the classifier (mean ± SD across 20 decoding runs). For visualization purposes here, feature selection was applied at each time point to data from all subjects to choose selective electrodes in the training data to be used in the classifier (**Methods**). Chance = 1/13, horizontal dashed line.

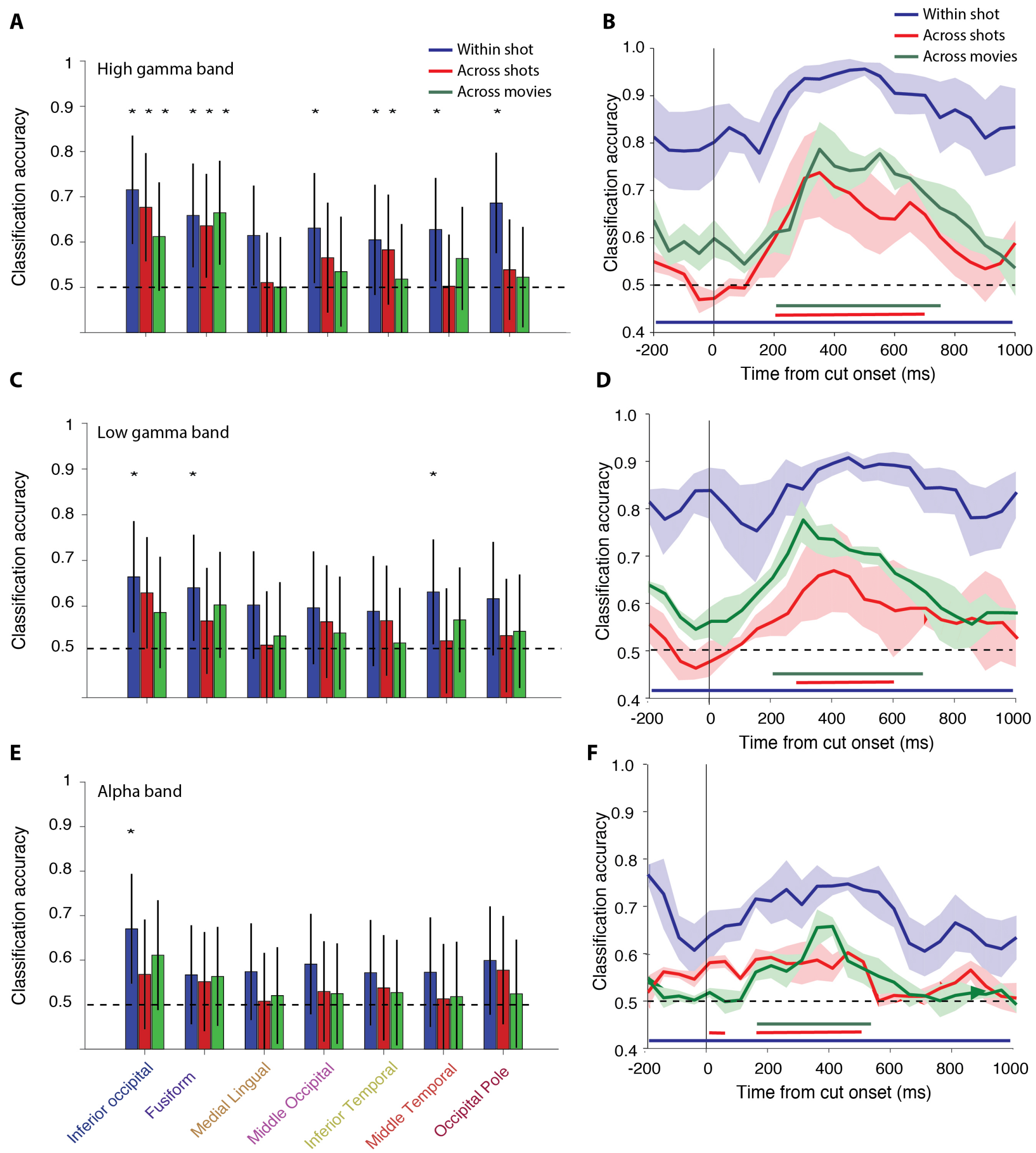

Supplemental Figure 9 – Visual information generalizes across movies in 12s clips using gamma band signals [expanding on Figure 5] This figure follows the format of **Figure 5B-C**, using here the signals in the high-gamma band (**A, B**), low-gamma band (**C, D**) and alpha band (**E, F**). **A, C, E**. Classification accuracy from n=8 electrodes in each region for shots with an animal versus shots without an animal in the 7 regions highlighted in **Fig. 4A** (mean ± SD across 20 decoding runs). The classification accuracy is reported as the average from 50-400 ms post cut onset. We considered 3 conditions corresponding to different levels of extrapolation: within shot (blue), across shots (red), and across movies (green). Asterisks indicate significant decoding for each of the three decoding conditions based on p<0.01 permutation test. Chance = 0.5, horizontal dashed line.
B, D, F. Visualization of dynamic classification accuracy for shots with an animal versus no animal across time relative to cut onset from a pseudo population across all subjects and electrodes (mean ± SD across 20 decoding runs). Feature selection was applied at each time point using data from all subjects to choose selective electrodes in the training data to be used in the classifier (Methods). Horizontal line indicates chance classification. Note that the 'within shot' classification accuracy was above chance levels even before cut onset, because the visual stimulus pre-cut was identical in the training and test sets. The horizontal bars denote the time periods of statistical significance.

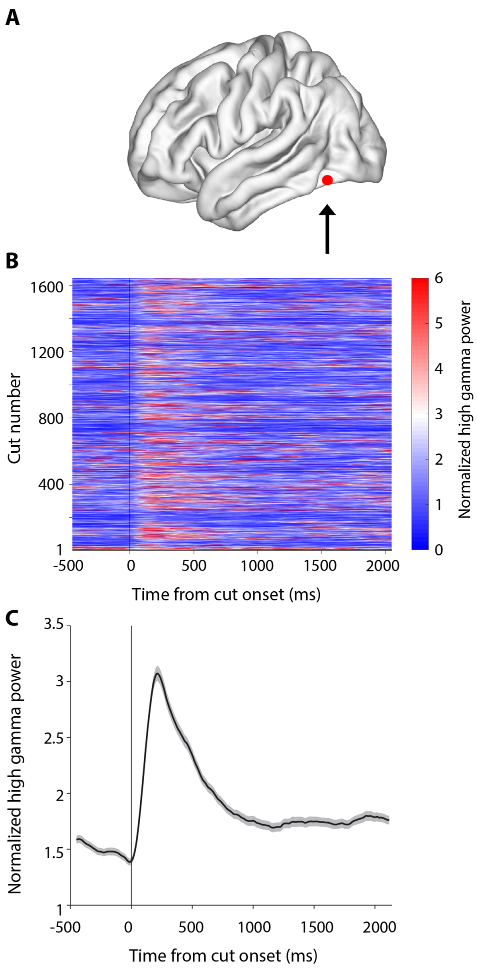

Supplemental Figure 10 – Example electrode showing a consistent physiological response in the high gamma band to movie cuts in Experiment II [expanding on Figure 6]

A. Location of an example cut-responsive electrode in the left middle occipital gyrus (Talairach coordinates = [-26.6 -79.1 -12.9]) based on the 70-120 Hz responses.

B. Raster plot showing the normalized high gamma power surrounding all cut transitions in the full-length movie (similar format to **Fig. 6B**). Each row denotes a repetition of the movie (n=1630 movie cuts, bin size = 10 ms, see color scale on right).

C. Average normalized gamma band power (mean ± SEM) over all movie cuts.

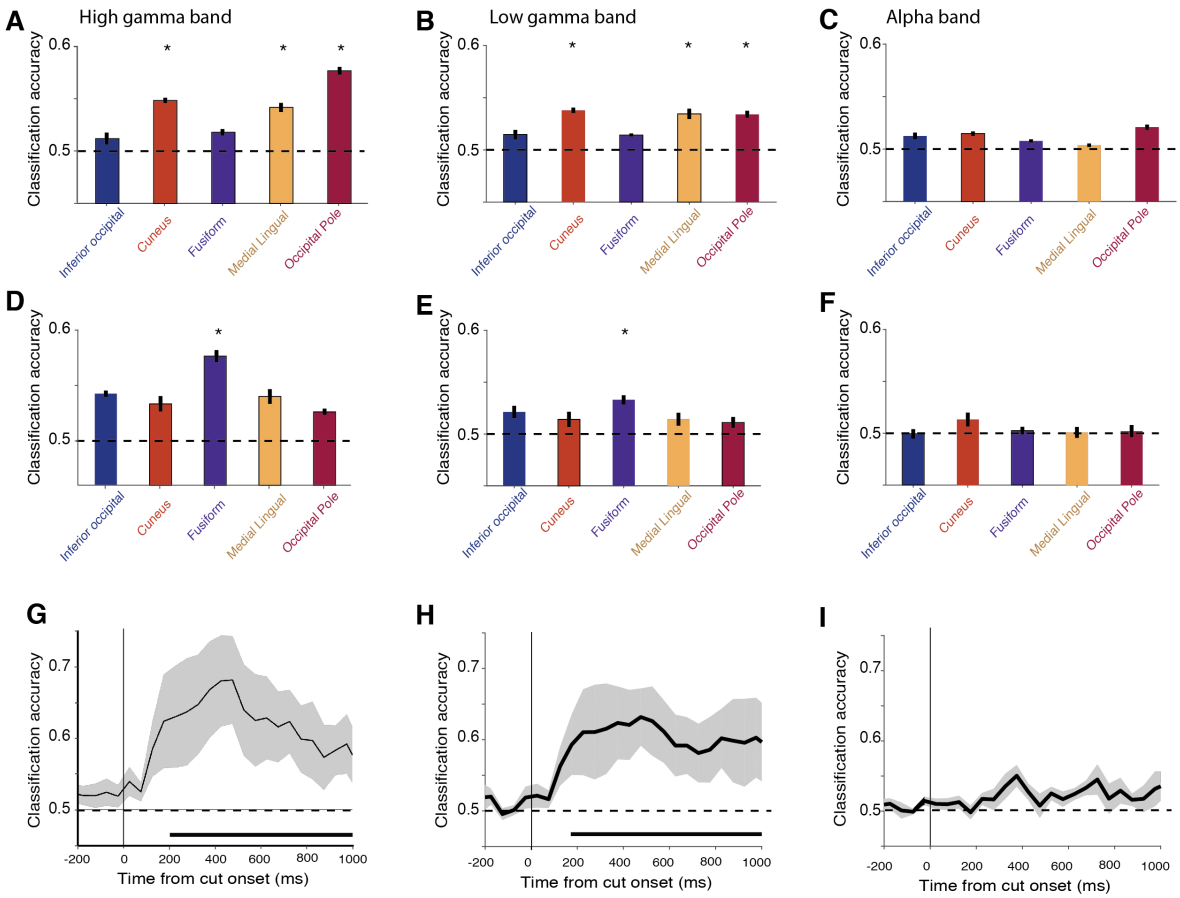

Supplemental Figure 11 – Decoding visual information in full-length movies in Experiment II [expanding on Figures 7]

Parts **A-C** follow the format of **Figure 7B**, parts **D-F** follow the format of **Figure 7C**, and parts **G-I** follow the format of **Figure 7D**, here shown using high gamma band (**A, D, G**), low gamma band (**B, E, H**) and alpha band (**C, F, I**) signals.

(**A-C**) Average single electrode classification accuracy between movie segments with a cut versus those without a cut for the 5 regions highlighted in **Figure 7A** (mean ± SEM across all electrodes in each region). Chance = 0.5 (horizontal dashed line). The classification accuracy is calculated as the average from 50-400 ms post cut onset. The number of electrodes averaged is shown in **Table S5**. Asterisks indicate regions with significantly above chance average classification accuracy based on a p<0.01 permutation test (**Methods**).

(D-F) Average single electrode classification accuracy between movie segments with a face versus those without a face for the 5 regions highlighted in **Figure 7A** (same format as **A-C**).

(G-I). Visualization of dynamic classification accuracy using gamma band signals as a function of time from cut onset for shots with a face versus no face from a pseudopopulation combining data from all subjects (mean ± SEM across four subjects). Feature selection was applied at each time point using data from all subjects to choose selective electrodes in the training data to be used in the classifier, (Methods). Since the subjects viewed different movies, decoding results were then averaged post-hoc. The horizontal dashed line indicates chance classification. Although classification seems to be slightly above chance prior to time zero, this was not statistically significant. The horizontal lines denotes those time periods of statistical significance.

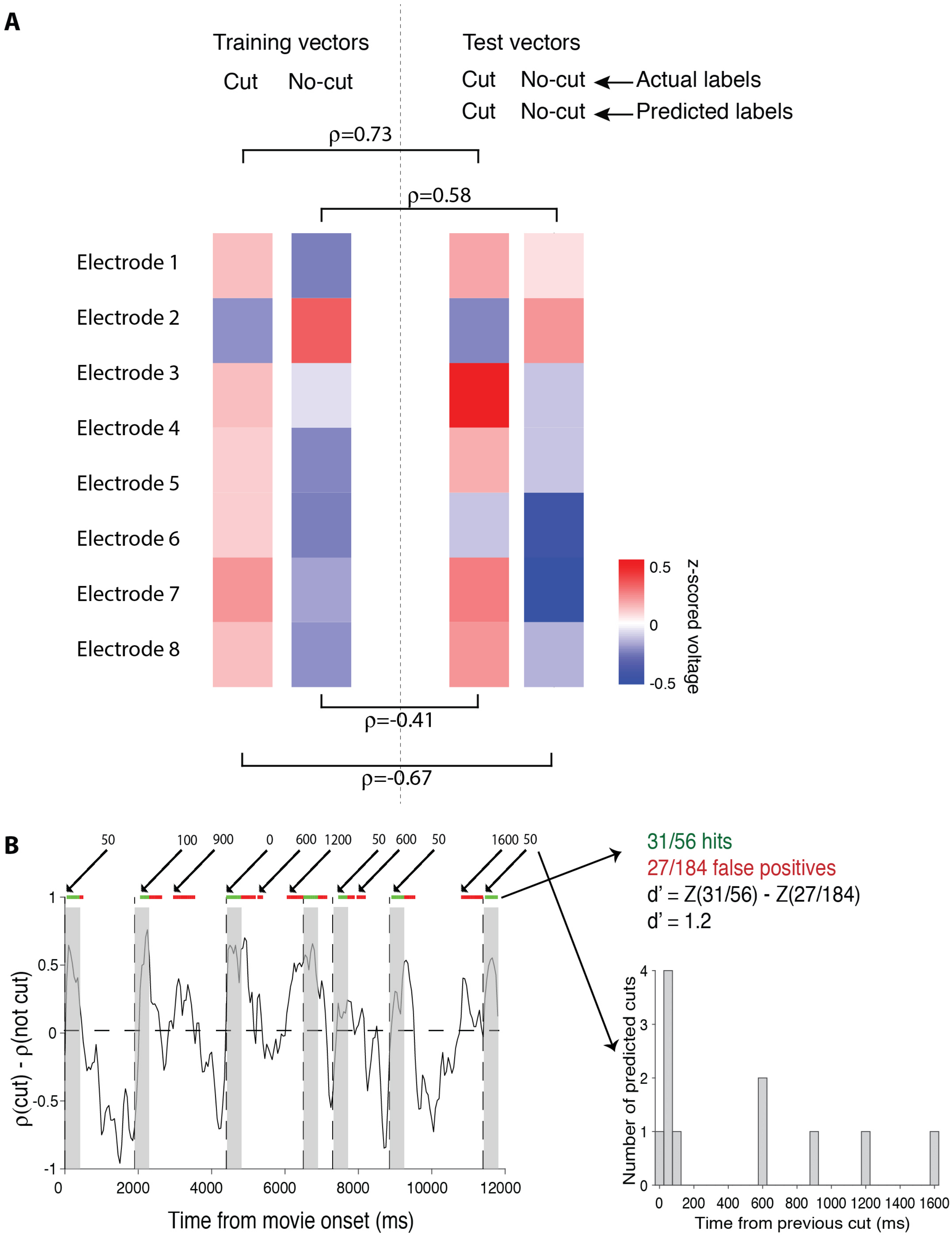
A
Training vectors
Cut
No-cut
Test vectors
Cut
No-cut
Actual labels
Cut
No-cut
Predicted labels
ρ=0.73
ρ=0.58
Electrode 1
Electrode 2
Electrode 3
Electrode 4
Electrode 5
Electrode 6
Electrode 7
Electrode 8
0.5
0
-0.5
z-scored voltage
ρ=-0.41
ρ=-0.67
B
50
100
900
0
600
1200
50
600
50
1600
50
31/56 hits
27/184 false positives
d' = Z(31/56) - Z(27/184)
d' = 1.2
ρ(cut) - ρ(not cut)
Time from movie onset (ms)
Number of predicted cuts
Time from previous cut (ms)

Supplemental Figure 12 – Illustration of correlation based classification procedure
(**A**) For illustration purposes, the data in this figure are derived from the inferior occipital gyrus, 200 ms post-cut onset time point in **Figure 4B**. In each trial, we compute the average voltage in a window of 50 ms for each of 8 electrodes. The normalized voltage (z-scored) is shown here (see color scale on the bottom right). On the left, we show the average activity pattern across 8 electrodes for the training data for the “cut” or “no-cut” labels. During testing, for each single event, we compute the correlation coefficient (ρ) with the two average training vectors. For the first test vector, the correlation coefficient with the “cut” training vector (0.73) is higher than the one for the “no-cut” one (-0.41), hence this event with be classified as “cut”. See **Methods** for further details.
(**B)** For illustration purposes, the data in this figure are derived from the fusiform gyrus in **Figure 4C**, movie 2. We calculate the training vectors for “cut” and “no cut” labels as in part **(A)** and average these vectors across the 0-400 ms post-cut onset period. For a held-out run, we correlate the activity in each 50 ms bin with the “cut” and “no cut” vector. The left panel of this figure shows a time course of the difference between these two correlation coefficients for one trial. Each bin is assigned a label of “+1” if the y axis is >0 and “-1” otherwise. Time bins that have a +1 label and are within 0 to 400 ms of a cut (time windows highlighted in gray), are considered hits and are marked by a green horizontal line on top. Time bins that have a +1 label and are beyond 400 ms of a cut are considered false alarms and are marked by a red horizontal line on top. There are 12000 ms / 50 ms = 240 bins, of these 56 bins (7x400 ms / 50 ms) that are within 0 to 400 ms of a cut and 184 bins that are not. In this example trial, the algorithm finds 31 hits (hit rate = 31/56) and 27 false alarms (false alarm rate = 27/184). We quantify the performance of the algorithm by computing d’=Z(hit rate)-Z(false alarm rate) where Z is the inverse of the cumulative distribution function (top right).
Second, we estimate how far away the predicted visual transitions fall from actual cuts, by taking the first time bin in a continuous segment classified as +1 above (shown above with arrows in the panel on the left) and measuring its distance to the previous true cut. The time is shown above each arrow and the panel on the right shows a histogram of these times for example trial. See **Methods** for further details.

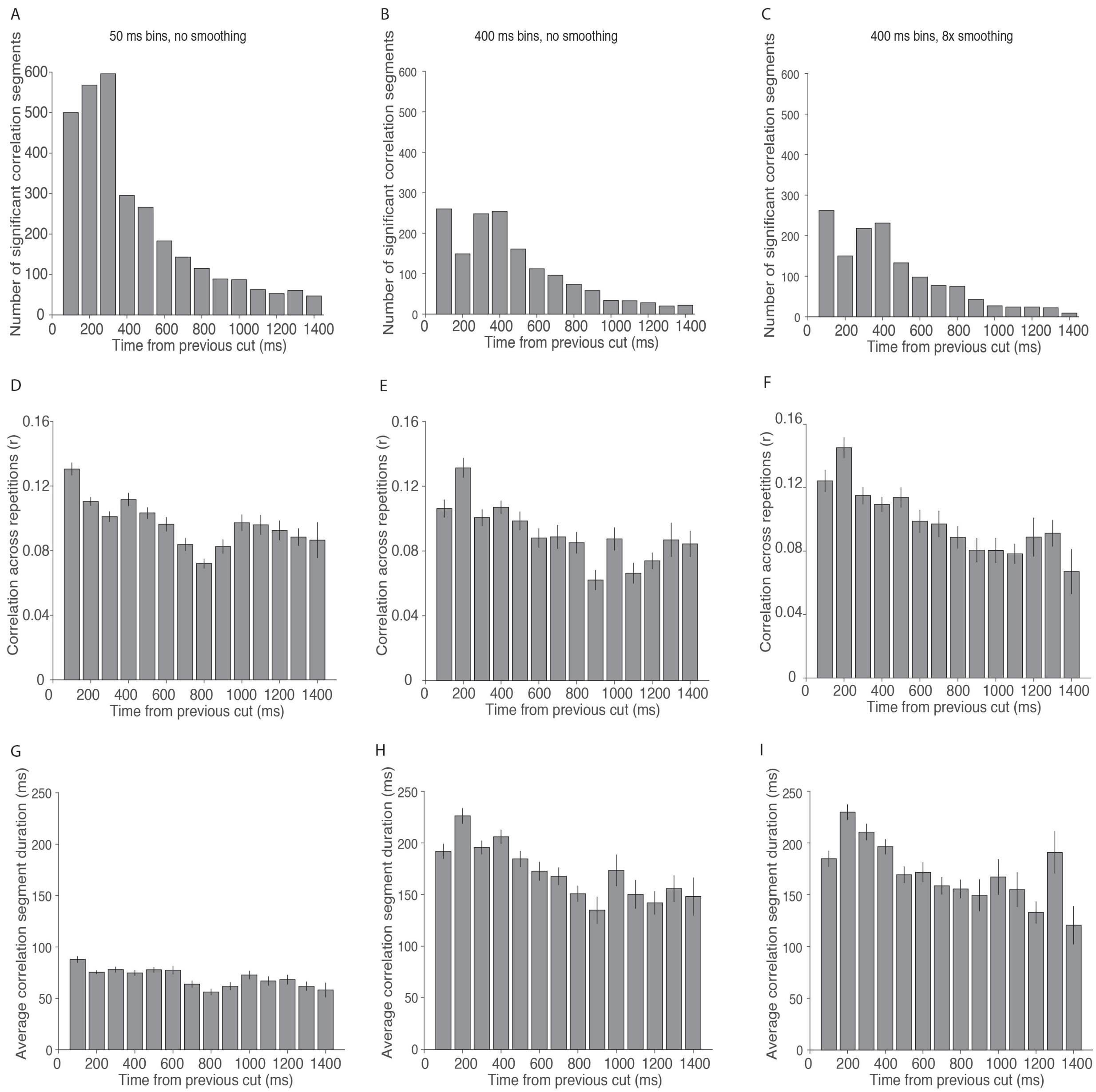

Supplemental Figure 13 – Properties of neural responses that were consistent across trials at different time scales [expanding on Figure 3]

A, D, G. Reproduction of panels in **Figures 3A-C** for comparison purposes. Note that the scale of the y-axis in **G** was changed for comparison with **H**, **I**.

B, **E**, **H**. Same as A, D, G, calculated using a 400 ms window instead of a 50 ms window. Because of the longer time windows, many such windows overlapped a movie cut and these were removed from the analyses to avoid confusing correlations during inter-cut segments with those elicited by movie cuts.

C, **F**, **I**. Same as B, E, H (window size of 400 ms) but resampling the data with a smoothing factor of 8 such that the number of time points contributing to the computation of correlation coefficients was the same in **C**, **F**, **I** and **A**, **D**, **G**. Windows overlapping movie cuts were excluded from these analyses.

2. Supplementary Tables

Subject number	Number of electrodes	Sampling Rate (Hz)	Number of repetitions	Number of repetitions	Number of repetitions
			Movie 1	**Movie 2**	**Movie 3**
1	72	500	59	59	59
2	104	256	26	26	18
3	88	256	42	42	21
4	72	256	68	68	34
5	88	500	60	60	30
6	74	256	24	24	12
7	96	256	22	22	11
8	112	256	20	20	10
9	88	256	20	20	10
10	96	256	38	38	19
11	64	256	32	32	16
TOTALS	**954**				

Table S1: Additional data for experiment I. Number of electrodes, sampling rate and number of repetitions for each movie in experiment I.

Subject number	# electrodes	# Cut responsive electrodes Broad band	# Cut responsive electrodes High gamma	Overlap with broad band #	Overlap with broad band %	# Cut responsive electrodes Low gamma	Overlap with broad band #	Overlap with broad band %	# Cut responsive electrodes Alpha	Overlap with broad band #	Overlap with broad band %
1	72	9	11	7	78%	3	2	22%	7	7	78%
2	104	4	3	3	75%	1	1	25%	0	0	0%
3	88	9	6	2	22%	14	7	78%	4	4	44%
4	72	0	0	0		0	0		0	0	
5	88	5	5	3	60%	1	0	0%	2	2	40%
6	74	0	0	0		1	0		1	0	
7	96	1	2	0	0%	0	0	0%	1	0	0%
8	112	6	6	3	50%	9	5	83%	1	1	17%
9	88	5	4	4	80%	1	1	20%	2	2	40%
10	96	1	0	0	0%	0	0	0%	3	0	0%
11	64	11	9	5	45%	2	2	18%	7	5	45%
TOTALS	**954**	**51**	**46**	**27**	**53%**	**32**	**18**	**35%**	**28**	**21**	**41%**

Table S2. Number of cut responsive electrodes in different frequency bands (Experiment I). For each subject, we report here the number of cut responsive electrodes using broadband signals (column 3, as reported in the main text), as well as in the high gamma band, low gamma band, and alpha band signals. For each frequency band, we report the degree of overlap with the broadband electrodes. The degrees of overlap between the responsive electrodes in different frequency bands and the ones in the broadband voltage were highly significant (p=0.0001). To assess statistical significance, we conducted 10,000 random draws of the number of responsive electrodes in each frequency band and evaluated the degree of overlap with the cut responsive electrodes defined by the broadband signals in each draw. Across these 10,000 runs, the maximum number of overlapping electrodes was 13 (high gamma), 9 (low gamma), and 9 (alpha), which were well below the actual number of overlapping electrodes (27, 18 and 21 respectively).

Subject number	# electrodes	Sampling rate (Hz)	# Cut responsive electrodes Broadband	# Cut responsive electrodes High gamma	Overlap with broadband #	Overlap with broadband %	# Cut responsive electrodes Low gamma	Overlap with broadband #	Overlap with broadband %	# Cut responsive electrodes Alpha	Overlap with broadband #	Overlap with broadband %
12	72	500	13	10	4	31%	3	3	23%	1	0	0%
13	144	2000	36	30	18	50%	14	14	39%	0	0	0%
14	26	500	1	0	0	0%	4	0	0%	1	1	100%
15	88	2000	11	12	7	64%	3	2	18%	2	1	9%
TOTALS	**330**		**61**	**52**	**29**	**48%**	**24**	**19**	**31%**	**4**	**2**	**3%**

Table S3. Number of cut responsive electrodes in different frequency bands (Experiment II). For each subject, we report here the number of cut responsive electrodes using broadband signals (column 4, as reported in the main text), as well as in the high gamma band, low gamma band, and alpha band signals. For each frequency band, we report the degree of overlap with the broadband electrodes (Methods). We followed the procedure described in Table S2 to evaluate the statistical significance of the degree of overlap. The degree of overlap between the responsive electrodes when considering the high and low gamma power and the broadband voltage were highly significant (p=0.0001). Out of 10,000 random draws we obtained at most 21 (high gamma) and 12 (low gamma) electrodes which were well below the actual number of overlapping electrodes (29 and 19 respectively). The degree of overlap when considering signals in the alpha power and broadband voltage was not statistically significant (p=0.07).

Region	Total electrodes	# subjs	Num. cut responsive Broad band	# subjs	% Cut responsive	Num. cut responsive High Gamma	# subjs	% Cut responsive	Num. cut responsive Low gamma	# subjs	% Cut responsive	Num. cut responsive Alpha	# subjs	% Cut responsive
Fronto-marginal	6	2	0	0	0.0%	0	0	0.0%	0	0	0.0%	0	0	0.0%
Inferior occipital	17	7	12	5	70.6%	8	4	47.1%	2	2	11.8%	8	4	47.1%
Sub-central gyrus	28	8	1	1	3.6%	0	0	0.0%	0	0	0.0%	0	0	0.0%
Transverse frontal pole	7	2	0	0	0.0%	0	0	0.0%	0	0	0.0%	0	0	0.0%
Cingulate post-dorsal	5	2	0	0	0.0%	0	0	0.0%	0	0	0.0%	0	0	0.0%
Cingulate post-ventral	6	2	1	1	16.7%	1	1	16.7%	1	1	16.7%	0	0	0.0%
Cuneus	13	3	0	0	7.7%	1	1	7.7%	0	0	0.0%	0	0	0.0%
Frontal inferior - Opercular	20	8	1	1	5.0%	1	1	5.0%	1	1	5.0%	0	0	0.0%
Frontal inferior - Orbital	7	5	0	0	0.0%	0	0	0.0%	0	0	0.0%	0	0	0.0%
Frontal inferior -Triangular	30	7	0	0	0.0%	0	0	0.0%	0	0	0.0%	0	0	0.0%
Frontal middle	37	6	0	0	0.0%	0	0	0.0%	0	0	0.0%	0	0	0.0%
Frontal superior	11	4	0	0	0.0%	0	0	0.0%	0	0	0.0%	0	0	0.0%
Insula	2	1	0	0	0.0%	0	0	0.0%	0	0	0.0%	0	0	0.0%
Fusiform	39	7	5	4	17.9%	4	4	10.3%	4	2	10.3%	2	2	5.1%
Medial lingual	33	6	5	1	18.2%	4	2	12.1%	7	2	21.2%	2	2	6.1%
Parahippocampal	27	8	1	1	0.0%	1	1	3.7%	2	2	7.4%	0	0	0.0%
Middle occippital	24	6	7	3	29.2%	5	3	20.8%	4	2	16.7%	4	2	16.7%
Occipital superior	8	2	0	0	12.5%	1	1	12.5%	0	0	0.0%	0	0	0.0%
Orbital gyrus	44	7	0	0	0.0%	0	0	0.0%	0	0	0.0%	0	0	0.0%
Inferior parietal - angular	33	6	0	0	0.0%	0	0	0.0%	0	0	0.0%	0	0	0.0%
Inferior parietal - supramarignal	36	8	1	1	0.0%	0	0	0.0%	0	0	0.0%	0	0	0.0%
Superioer parietal	4	3	0	0	0.0%	0	0	0.0%	0	0	0.0%	0	0	0.0%
Postcentral gyrus	23	7	0	0	0.0%	0	0	0.0%	0	0	0.0%	0	0	0.0%
Precentral Gyrus	22	8	1	1	0.0%	0	0	0.0%	0	0	0.0%	0	0	0.0%
Precuneus	15	1	0	0	0.0%	0	0	0.0%	0	0	0.0%	0	0	0.0%
Gyrus rectus	7	3	0	0	0.0%	0	0	0.0%	0	0	0.0%	0	0	0.0%
Lateral temporal superior	75	10	1	1	1.3%	0	0	0.0%	1	1	1.3%	0	0	0.0%
Superior temporal gyrus - polar	3	2	0	0	33.3%	1	1	33.3%	0	0	0.0%	0	0	0.0%
Superior temp gyrus - temporal	2	2	0	0	0.0%	0	0	0.0%	0	0	0.0%	0	0	0.0%
Inferior Temporal	92	10	5	2	7.6%	3	2	3.3%	3	1	3.3%	2	1	2.2%
Middle Temporal	107	11	3	2	2.8%	2	2	1.9%	0	0	0.0%	1	1	0.9%
Occipital pole	9	3	5	2	88.9%	8	2	88.9%	2	1	22.2%	3	2	33.3%
Temporal pole	38	9	0	0	0.0%	1	1	2.6%	2	2	5.3%	0	0	0.0%
Calcarine sulcus	2	1	0	0	0.0%	0	0	0.0%	0	0	0.0%	0	0	0.0%
Inferior insula	1	1	0	0	0.0%	0	0	0.0%	0	0	0.0%	0	0	0.0%
Anterior collateral sulcus	7	5	0	0	0.0%	0	0	0.0%	1	1	14.3%	0	0	0.0%
Posterior collateral sulcus	1	1	1	1	100%	1	1	100%	0	0	0.0%	0	0	0.0%
Frontal inferior sulcus	3	2	0	0	0.0%	0	0	0.0%	0	0	0.0%	0	0	0.0%
Frontal middle sulcus	1	1	0	0	0.0%	0	0	0.0%	0	0	0.0%	0	0	0.0%
Intermediate parietal sulcus of Jensen	1	1	0	0	100%	1	1	100%	0	0	0.0%	0	0	0.0%
Orbital sulcus (H-shaped)	8	5	0	0	0.0%	0	0	0.0%	0	0	0.0%	0	0	0.0%
Lateral orbital sulcus	1	1	0	0	0.0%	0	0	0.0%	0	0	0.0%	0	0	0.0%
Parieto-occipital sulcus	8	1	0	0	0.0%	0	0	0.0%	0	0	0.0%	0	0	0.0%
Sub-parietal sulcus	2	1	0	0	0.0%	0	0	0.0%	0	0	0.0%	0	0	0.0%
Inferior temporal sulcus	2	2	0	0	0.0%	0	0	0.0%	0	0	0.0%	0	0	0.0%
Superior temporal sulcus	7	5	0	0	14.3%	1	1	14.3%	0	0	0.0%	0	0	0.0%
Unknown	80	9	1	1	1.3%	2	2	2.5%	2	2	2.5%	6	2	7.5%
TOTALS	**954**		**51**		**5.3%**	**46**		**4.8%**	**32**		**3.4%**	**28**		**2.9%**

Supplemental Table 4 – List of electrode locations and number of cut-responsive electrodes in each region (Experiment I)

We report the number of cut-responsive electrodes using the broadband signals (as reported in the main text) or using IFP signals filtered in the high gamma, low gamma or alpha frequency bands. In each case, we report the number of subjects where those electrodes came from. Colored regions correspond to the locations highlighted in **Figure 4A**. Regions shaded in gray indicate locations with >= 8 electrodes that were used in the decoding analysis, but did not yield statistically significant classification accuracy in the analyses in **Figures 4** or **5B**.

Region	Total electrodes	# subjs	Num. cut responsive Broadband	# subjs	% Cut responsive	Num. cut responsive High Gamma	# subjs	% Cut responsive	Num. cut responsive Low gamma	# subjs	% Cut responsive	Num. cut responsive Alpha	# subjs	% Cut responsive
Inferior occipital	7	3	2	1	28.6%	1	1	14.3%	0	0	0.0%	0	0	0.0%
Subcentral gyrus	7	2	2	2	28.6%	1	1	14.3%	0	0	0.0%	1	1	14.3%
Cingulate gyrus post-dorsal	16	1	1	1	6.3%	2	1	12.5%	0	0	0.0%	0	0	0.0%
Cingulate gyrus post-ventral	4	1	0	0	0.0%	0	0	0.0%	0	0	0.0%	0	0	0.0%
Cuneus	10	2	8	2	80.0%	4	1	40.0%	5	1	50.0%	1	1	10.0%
Frontal inferior - Opercular	8	2	2	1	25.0%	1	1	12.5%	0	0	0.0%	0	0	0.0%
Frontal inferior - Orbital	4	2	0	0	0.0%	0	0	0.0%	0	0	0.0%	0	0	0.0%
Frontal inferior -Triangular	7	2	2	1	28.6%	0	0	0.0%	0	0	0.0%	0	0	0.0%
Fusiform gyrus	26	4	10	2	38.5%	14	3	53.8%	2	1	7.7%	0	0	0.0%
Medial lingual gyrus	11	3	6	1	54.5%	7	2	63.6%	5	2	45.5%	0	0	0.0%
Parahippocampal	22	3	0	0	0.0%	0	0	0.0%	1	1	4.5%	1	1	4.5%
Occipital middle	14	2	1	1	7.1%	1	1	7.1%	0	0	0.0%	0	0	0.0%
Occipital superior	5	2	0	0	0.0%	1	1	20.0%	0	0	0.0%	0	0	0.0%
Orbital gyrus	14	2	1	1	7.1%	2	1	14.3%	0	0	0.0%	0	0	0.0%
Inferior parietal - angular	6	1	2	1	33.3%	1	1	16.7%	0	0	0.0%	0	0	0.0%
Inf parietal - supramarignal	3	1	0	0	0.0%	0	0	0.0%	0	0	0.0%	0	0	0.0%
Superioer parietal	2	1	0	0	0.0%	0	0	0.0%	0	0	0.0%	0	0	0.0%
Precentral gyrus	2	1	1	1	50.0%	0	0	0.0%	0	0	0.0%	0	0	0.0%
Precuneus	35	1	11	1	31.4%	6	1	17.1%	2	1	5.7%	0	0	0.0%
Lateral temporal superior	23	3	3	1	13.0%	3	3	13.0%	2	2	8.7%	1	1	4.3%
Sup temp gyrus - temporal	1	1	0	0	0.0%	0	0	0.0%	0	0	0.0%	0	0	0.0%
Temporal inferior	26	3	2	1	7.7%	0	0	0.0%	0	0	0.0%	0	0	0.0%
Temporal middle	37	3	1	1	2.7%	1	1	2.7%	0	0	0.0%	0	0	0.0%
Medial wall	3	1	0	0	0.0%	0	0	0.0%	0	0	0.0%	0	0	0.0%
Occipital pole	13	2	3	1	23.1%	3	1	23.1%	5	2	38.5%	0	0	0.0%
Temporal pole	15	2	2	1	13.3%	3	1	20.0%	2	1	13.3%	0	0	0.0%
Medial lingual sulcus	2	2	1	1	50.0%	0	0	0.0%	0	0	0.0%	0	0	0.0%
Orbital sulcus (H-shaped)	5	2	0	0	0.0%	1	1	20.0%	0	0	0.0%	0	0	0.0%
Superior temporal sulcus	2	1	0	0	0.0%	0	0	0.0%	0	0	0.0%	0	0	0.0%
TOTALS	**330**		**61**		**18.5%**	**52**		**15.8%**	**24**		**7.3%**	**4**		**1.2%**

Supplemental Table 5 – List of electrode locations (Experiment II)
Number of electrodes in each region. We report the number of cut-responsive electrodes using the broadband and the gamma band signals with the number of subjects that the electrodes came from indicated in parentheses. Colored regions correspond to the locations highlighted in **Figure 7A**. Regions shaded in gray indicate locations with >= 5 electrodes that did not yield statistically significant classification accuracy in the analyses in **Figures 7B** or **8A**.

3. Supplementary Discussion

In contrast to action potentials, the biophysical origin of field potential signals is poorly understood (Buzsaki et al 2012, Nature Reviews Neuroscience). In particular, it is interesting to examine the response properties of intracranial field potential signals filtered in different frequency bands. Several studies have demonstrated that different frequency bands of the IFP signals are typically correlated but are certainly not identical (e.g. (Canolty et al. 2006; Vidal et al. 2010; Bansal et al. 2012; Miller et al. 2014)). In those studies, as well as ours, the frequency bands examined refer to *broadband* ranges, as opposed to oscillations at a single frequency.

In the main text, we focused on the analyses of "raw" unfiltered broadband signals. Here we re-examined the responses after filtering the IFP signals in different frequency bands. Specifically, we considered broadband high-gamma signals (70 – 120 Hz), broadband low-gamma signals (25 – 70 Hz) and broadband alpha signals (8 – 15 Hz). The conclusions were qualitatively and conceptually similar when considering different frequency bands. As expected, there were quantitative differences in terms of the number of responsive electrodes, the performance of the different types of classifiers, etc. Here we provide a detailed description and discussion of the results in different frequency bands and how they compare to those reported using unfiltered broadband signals. We follow the structure in the main text.

3.1 - Neurophysiological responses to time-varying stimuli (Experiment I)

We observed cut-responsive electrodes in other frequency bands, similar to the example electrode depicted in **Figure 2**. **Figure S2** shows an example electrode that demonstrates modulation triggered by movie cuts in the high gamma band. In all, we observed 46, 32 and 28 cut-responsive electrodes in the high gamma, low gamma and alpha bands, respectively (Table S2 describes the distribution among the different subjects). Of these, 27 (53%), 18 (35%) and 21 (41%) overlapped with the 51 cut-responsive electrodes described in the main text. To assess whether this degree of overlap could be obtained by chance, we considered 10,000 iterations where we randomly drew the corresponding number of electrodes in each frequency band and each subject and re-calculated the degree of overlap. Even though the degree of overlap was well below 100%, it was still highly significant ($p<0.0001$) in all three frequency bands. The brain areas where we observed most cut-responsive electrodes in the broadband signals were also generally the brain areas that led to more cut-responsive electrodes in the different frequency bands (**Table S4**).

3.2 – Responses that were reproducible between repetitions largely clustered shortly after movie cuts

When examining the entire 12s clips, we noted that those responses in the broadband signals that were reproducible across repetitions were largely clustered in the vicinity after movie cuts, were stronger shortly after movie cuts and had longer durations when they happened shortly after movie cuts. These conclusions were confirmed in the different frequency bands (**Figure S3**), with the exception of the alpha band signals that did not show a clear decrease in correlation strength with time from previous cut (**Figure S3F**).

3.3 - Detecting the presence of movie cuts (Experiment I)

We could detect the presence or absence of a movie cut in single events using signals in the high-gamma band or low-gamma band (**Figure S7A-B**), as reported for the broadband signals in **Figure 4B**. The results were weaker in the alpha band where only one region (middle occipital gyrus) showed marginal, but statistically significant, classification accuracy. The mean classification accuracy was 0.60±0.05 (mean±SD) in the high-gamma band and 0.56±0.1 in the low-gamma band. The overall classification accuracies in the 5 regions highlighted in **Figure 4B** were similar, though slightly lower, when considering the gamma band signals. However, there were two regions, the medial lingual gyrus and the middle temporal gyrus that reached statistically significant classification accuracy when considering the gamma band signals but not when considering the broadband signals (compare **Figure 4B** versus **S7A-B**). The inferior occipital gyrus, fusiform gyrus and middle temporal gyrus showed significant classification performance in the broadband signals but not in the low-gamma signals.

We next evaluated whether we could detect visual transitions in single events during the entire 12s clips in the different frequency bands (**Figure S7D-F**). Classifiers using data in the high gamma band detected transitions with above chance precision with data from three of the seven regions (inferior occipital gyrus, medial lingual gyrus, and middle occipital gyrus). The average d' across these three regions was 0.47±0.25 (mean±SD). Classifiers using data in the low gamma band also detected transitions with above chance precision in three of the seven regions (fusiform gyrus, medial lingual gyrus, and middle occipital gyrus). The average d' across these three regions was 0.4±0.08. Classifiers using data in the alpha band detected transitions significantly above chance in two regions (inferior occipital and inferior temporal). The average d' across these three regions was 0.39±0.1. The regions identified in each of these frequency bands represent a subset of those identified with the broadband voltage signals (see **Figure 4C**).

We estimated the latency of the visual transition predictions in each of the regions that passed the significance criterion in **Figures S7D-F** by measuring the time difference to the nearest prior cut (**Figure S7G-I**). The distribution of these time differences was significantly different from the one expected under the null hypothesis defined by 10,000 runs of randomly selecting the same number of time points per movie as predicted transitions (**Figure S7G-I**, black line, $p<10^{-7}$, $p<10^{-10}$, $p<10^{-8}$, for high gamma, low gamma, and alpha bands, respectively based on Kolmogorov-Smirnov test).

3.4 - Decoding visual events in movies (Experiment I)

When using different IFP signals in different frequency bands to discriminate among the 13 movie cuts, the results were similar to those reported in the main text (compare **Figure S8A-C** with **Figure 5B**). The fusiform gyrus did not show significant performance for the low-gamma band or alpha band and the medial lingual gyrus did not show significant performance in the alpha band. The mean classification accuracies were 0.20±0.05 for the high gamma band 0.18±0.04 for the low-gamma band and 0.18±0.05 for the alpha band (compared to 0.27±0.07 in the broadband signals). The dynamics obtained when considering a pseudopopulation across all brain regions were also qualitatively similar (**Figure S8D-G**).

3.5 - Invariant decoding of visual events in movies (Experiment I)

When considering whether we could extrapolate across different shots or event different movie clips to assess the degree of invariance in the underlying representation, the results obtained for the high-gamma band signals were quite similar to those in the broadband signals (compare **Figure S9A** versus **Figure 5C**). The only qualitative differences were that the inferior temporal gyrus and the occipital pole showed significantly more invariance in the broadband signals. Quantitatively, the mean classification accuracy for the high-gamma signals was 0.65±0.04, slightly below the value of 0.74±0.06 reported for the broadband signals. Signals in the low-gamma and alpha bands within the seven regions discussed in **Figure 4A** demonstrated no invariance (**Figure S9C** and **S9E**).

3.6 - Detecting the presence of movie cuts in single presentation of movies (Experiment II)

We observed cut-responsive electrodes in the high-gamma and low-gamma bands, similar to the example electrode depicted in **Figure 6** for the broadband signals. **Figure S10** shows an example cut-responsive electrode when considering signals in the high-gamma band. In all, we observed 52, 24 and 4 cut-responsive electrodes in the high-gamma, low-gamma and alpha bands (**Table S3** shows the number of cut-responsive electrodes in each frequency band separately by subject). Of these, 29 (48%), 19 (31%) and 2 (3%) electrodes overlapped with the 61 electrodes reported in the broadband signals. The degree of overlap was highly significant for the high-gamma and low-gamma band responses ($p<0.0001$), but not for the alpha band responses. The locations that yielded more cut-responsive electrodes in the broadband signals were also overrepresented in the high-gamma and low-gamma band signals (**Table S4**).

We could decode the presence or absence of a movie cut using IFP signals filtered both in the high and low gamma bands in three of the four regions identified in **Figure 7A-B**: cuneus, medial lingual gyrus and the occipital pole (**Figure S11A-B**).

3.7 - Invariant decoding of visual events in single presentation of movies (Experiment II)

Considering both the high and low gamma band signals, the fusiform gyrus was the only region that reached significant classification accuracy in discriminating the presence of a face (**Figure S11D-E**) whereas the inferior occipital gyrus also showed significant decoding in the broadband signals (**Figure 7C**). The dynamics visualized in **Figures S11G-H** are similar to those rendered for the broadband signals in **Figure 7D**.